Journal of Archaeological Science, Volume 108, August 2019, Article number 104974
DOI:10.1016/j.jas.2019.104974

A unique recipe for glass beads at Iron Age Sardis

Alicia Van Ham-Meert[1,2], Sarah Dillis[1], Annelore Blomme[1], Nicholas Cahill[3], Philippe Claeys[2], Jan Elsen[1], Katherine Eremin[4], Axel Gerdes[5], Christian Steuwe[6], Maarten Roeffaers[6], Andrew Shortland[7], Patrick Degryse[1, 8]

[1] Earth and Environmental Science, Centre for archaeological Science, KU Leuven, Celestijnenlaan 200E, B-3001 Heverlee, Belgium

[2] Analytical, Environmental and Geochemistry, Vrije Universiteit Brussel, Triomflaan 2, B-1050 Elsene, Belgium

[3]Department of Art History, University of Wisconsin-Madison, 800 University Avenue Madison, WI 53706, USA

[4]Harvard Art Museums, 32 Quincy Street, Cambridge, MA 02138, USA

[5]Institut für Geowissenschaften, Abt. Petrologie und Geochemie, Altenhöferallee 1, D-60438 Frankfurt, Germany

[6]Centre for Surface Chemistry and Catalysis, KU Leuven, Celestijnenlaan 200F, 3001 Leuven, Belgium.

[7]Centre for Archaeological and Forensic Analysis, Department of Materials and Applied Sciences, Cranfield University, Shrivenham, Swindon SN6 8LA, UK

[8] Department of Archaeological Sciences, Faculty of Archaeology, Leiden University, Einsteinweg 2, 2333 CC Leiden, the Netherlands

Abstract

In large parts of the Mediterranean recipes for the earliest man-made glass changed from melting mixtures of crushed quartz pebbles and halophytic plant ashes in the Late Bronze Age to the use of quartz sands and mineral soda during the Early Iron Age. Not much is known about this transition and the experimental materials which would inevitably have been connected to such technological change. In this paper we present a unique snapshot of developments in glass technology in Anatolia during the Middle Iron Age, when glass is still a relatively rare commodity. The present work focusses on black glass beads decorated with yellow trails from eighth to seventh century BCE Sardis, glass beads that are very rare for this period, and on this site. A full elemental analysis of the beads was made, and Sr, Pb and B isotope ratios were determined. This study reveals the use of a combination of a previously unknown source of silica and of mineral soda, giving rise to elevated (granite-like) Sr isotope signatures, as well as high alumina and B concentrations. The yellow trails of glass on the beads consist of lead-tin yellow type II, lead stannate, showing the earliest occurrence of this type of opacifier/colourant so far, predating any other findings by at least four centuries. The production of these glass beads may be local to Sardis and experimental in nature. It is therefore suggested that Sardis may have played its role in the technological development of the glass craft during the Iron Age.

1. Introduction

1.1 Archaeological context

This study discusses the analysis of four black glass beads with decorative yellow trails and dots , dated to the eighth to seventh century BCE, found at Sardis. The ancient city of Sardis is located at the edge of the Hermus (modern Gediz) river plain, at the foot of the Tmolus (modern Bozdağ) mountains in western Turkey (SI – S1). During the Iron Age, Sardis was the capital city of the Lydians, known for their gold, for their invention of coinage, textiles, and other luxuries. The early history and archaeology of the city, before the seventh century BCE, is imperfectly known due to only scattered literary sources

and a relative dearth of archaeological evidence. By the seventh and sixth centuries BCE, however, the Lydians had expanded their empire to control the gold-producing regions of northwest Anatolia, as well as Greek cities of the coast, and inland as far as Phrygia and the Halys (modern Kızılırmak) river, to become the major military and economic power in Asia Minor. In 547 BCE, Cyrus the Great of Persia conquered Sardis and incorporated it into the Achaemenid empire as one of the most important Achaemenid satrapal capitals. Sardis remained an important urban center throughout the Hellenistic, Roman, and late Roman periods. The seventh century CE saw a rapid decline in settlement of the lower city, although the acropolis remained an important stronghold for many centuries (Hanfmann et al., 1983; Cahill, 2010a).

The beads discussed in this article are almost spherical, 1.0-1.2 cm in diameter, with a central hole for stringing. They are made from black glass with applied yellow glass trails and dots: a wavy trail around the center of the bead, framed by straight trails at the top and bottom (Fig. 1). These beads are known as eye-beads. About a dozen similar beads have been found in other Lydian levels at different sectors at Sardis, and few are known from later, post-Lydian strata. The dating and find context of the beads is discussed in detail in the SI.

The aim of this research is to identify the recipe used to make these glass artefacts, based on their chemical, crystallographic/structural and isotopic composition. For this purpose, a combination of EPMA (Electron Probe Micro-Analysis), LA-ICP-MS (laser ablation - inductively coupled plasma mass spectrometry), XRD (X-Ray Diffraction), Raman spectroscopy and isotopic analysis was applied on the glass samples. These data are used to place the beads within the larger story of glass manufacture during the first millennium BCE, an era of particular interest as it is a time of change in technologies and raw materials of which many particulars are still unknown.

1.2 Early Glass

Glass was produced in a regular and controlled way from the mid-sixteenth century BCE onwards in major centres of the Late Bronze Age Mesopotamian and Mediterranean civilizations. Depending on the raw materials used, different glass compositional groups have been identified (e.g. Sayre and Smith, 1961). In the Late Bronze Age, 'high magnesium-potassium' or 'plant ash' glasses were widespread in Egypt, Mesopotamia and Greece (e.g. Sayre and Smith, 1961; Shortland and Eremin, 2006), and similar glass artefacts have been found on contemporary European sites (e.g. Hartmann et al., 1997; Varberg et al., 2015). This first glassmaking technology involved the fusion of two main ingredients: quartz pebbles and halophytic plant ashes.

The end of the Bronze Age, in the late second millennium BCE, is characterised by the collapse and disappearance of the great empires in the Aegean, Anatolia and the Levant (Dickinson, 2006). At this time glass became rare, perhaps suggesting a decline in glass production (Drew, 1993). The archaeological record registers an increasing number of glass finds again from the Iron Age onwards. Until the seventh century BCE, glass production was in a transition phase, with a continued use of traditional recipes and ingredients inherited from the Late Bronze Age, alongside the use of an increasing variety of glass formulae and raw materials (Rehren and Freestone, 2015, Conte et al., 2016a, 2016b). A significant innovation at the beginning of the first millennium BCE is the production of glasses with a new fluxing agent, i.e. natron, a very pure mineral alkali source from evaporite deposits. The first glasses produced with natron as flux exhibit a highly variable chemical composition, due to the use of less standardised recipes and technologies (Conte et al., 2016a). Some of the earliest examples of this new technology are the tenth century BCE core-formed glass vessels found in the Egyptian burial of Nesikhons (Schlick-Nolte and Werthmann, 2003). Other glass types typical of this

period are the black and cobalt blue natron glasses found at Pella in the Levant, Nimrud in Mesopotamia and various sites in Southwestern Europe (Reade et al., 2006, 2009; Gratuze and Picon, 2006; Gratuze, 2009; Arletti et al., 2011; Conte et al., 2016a, 2016b). These different 'low magnesium-potassium' or 'natron' glasses were the forerunners of the later large-scale Hellenistic and Roman natron glass.

Much of this early glass was opaque and strongly coloured in nature. Early glass technology is characterized by the presence of calcium and lead antimonate for the production of opaque white ($Ca_2Sb_2O_7$ or $CaSb_2O_6$) and yellow ($Pb_2Sb_2O_7$) glass. There are a few occurrences of tin-based opacifiers, mainly in the form of cassiterite (SnO_2) in white glasses as early as the thirteenth century BCE in Tell Ashkelon in the Levant (Toffolo et al., 2013) and in the eighth and seventh centuries BCE in Poland (Purowski et al., 2012). However, apart from these rare examples, it is generally accepted that the use of tin-based opacifiers such as lead stannate yellow (lead-tin yellow type II $PbSnO_3$, $PbSn_{1-x}Si_xO_3$) and tin oxide white (SnO_2) gradually increases during the second to first centuries BCE in glass production in Europe (glass beads found in Britain, France and Czechoslovakia; Tite et al., 2008). Antimony-based opacifiers continued to be used in the Roman world, but are gradually replaced by tin-based opacifiers by the fourth century CE, spreading from the eastern Mediterranean into northern Europe, to be used throughout the Roman and Byzantine Empires.

In recent years high alumina glasses have been identified in Western Anatolia (Dussubieux et al. 2010, Schibille, 2010, Rehren et al. 2015 and Swan et al. 2018), Bulgaria (Bugoi et al. 2016) and Italy (Neri et al. 2019). Most of these occurrences are connected to the Byzantine period, although in Pergamon high alumina glasses are found as early as the first century CE. Overall, this glass type is under-studied, not many examples are known, and compositional groups have not been refined. Two main groups were described in the glass of Pergamon: the first is dark blue HBAl glass (characterized by B around 1000ppm, Al_2O_3 around 9wt%, CaO around 5wt% and Sr around 300ppm), while the second is transparent HLiBAl glass (characterized by B around 1500ppm, Li around 300ppm, Al_2O_3 around 4-7 wt%, CaO around 8-11wt%) (Rehren et al. 2015). Swan et al. (2018) reports compositional groups which are similar but distinct. Of interest for our work is the dark blue glass of group 2 (characterised by B between 1000-2000ppm, Al_2O_3 between 9.5-11 wt% and Co between 100-500ppm). Likewise in the glass assemblage from Romania, a few high alumina glasses were found. Their B and Li content is unknown, but they are characterised by elevated Fe_2O_3 concentrations (around 3 wt%). The current consensus on high alumina glasses in the Eastern Mediterranean is that they were likely made in Western Anatolia, using local raw materials including borax deposits, from the first century CE onwards but with the main production situated during the Byzantine period. This glass was used alongside regular imported natron glass. When in the Levant natron glass production ceases by the eighth-ninth century CE, it is replaced by plant ash glass. This transition is not necessarily observed in the assemblages from Western Anatolia. There, high alumina glass becomes the main glass type. Much is still unknown about these high alumina-high boron glasses, especially on their origin and how production and distribution were organized. The present study contributes to that discussion by showing that high alumina, boron and lithium glass was present in Sardis long before the first century CE.

2 Materials and Methods

2.1 Materials

The list of samples studied can be found in Table 1. Samples Sa-01, Sa-02 and Sa-03 (illustrated in Fig. 1) were cut through, mounted in epoxy resin and polished using diamond paste. The yellow and black parts of sample Sa-04 were separated. Table 1 also specifies the typology of the beads and which analysis were performed on which sample.

Figure 1: Beads from Lydian Sardis, Sa-01 (a), Sa-02 (b), Sa-03 (c)

2.2 Methods

EPMA

A JEOL JXA-8530F Hyperprobe Field Emission Gun-Electron probe micro-analyser (FEG-EPMA; KU Leuven, Belgium) was used to obtain the major and minor element composition of the beads (indicated by 'a' in Table 2). Analysis were performed on carbon-coated samples, at 15 kV accelerating voltage, 100 nA beam current and 50 µm spot size to minimize migration of sodium and other volatile elements (Henderson, 1988). Five points were analysed to obtain an average value. Element peaks were measured for 20s to 70s depending on the element. Background was measured twice during 5s. The measuring procedure was calibrated with matrix-matched Corning archaeological reference glass A and validated with Corning glass B (Vicenzi et al., 2002). Raw data were corrected with ZAF correction procedure to process for matrix effects (Vicenzi et al., 2002). Relative analytical accuracy and precision for the elements analysed were better than 9%, and detection limits for the different elements were below 0.02%. The mounted samples were coated with carbon for the analysis.

LA-ICP-MS

Trace element analyses were carried out using a New Wave UV213 laser ablation system coupled to an Agilent 7500a inductively coupled plasma mass spectrometer (LA-ICP-MS; Cranfield University, UK) (indicated by 'b' in table 2). Samples were ablated under argon flow and analysed in spot mode with a laser diameter of 80 µm, repetition rates of 10 Hz and 15 $\mathrm{J \cdot cm^{-2}}$ fluence. Ablated material was transported to the plasma at 0.5 $l \cdot min^{-1}$ and the plasma was operated at a power of 1430 to 1470 W. The quantification was done using the sum normalization calibration technique (Van Elteren et al., 2009). All elements were normalized to 100% based on their corresponding oxide concentrations and the concentration of a particular major oxide, here SiO_2, as normalizing factor (Gratuze et al., 2001). External calibration of the ICP-MS data was performed utilising glass reference materials NIST SRM 610 and 612 (Pearce et al., 1997). Analytical uncertainties below 20% were obtained, limits of detection are reported in table 2. Corning glass A was measured to validate the measurements (results are also reported in table 2). The sample preparation consisted of removing the C-coating of the mounted sections used for EPMA.

XRD

The yellow part of sample Sa-04 was crushed in an agate mortar and placed on the XRD holder using silica gel. It was measured using a Phillips PW1830 diffractometer with a Bragg/Brentano θ - 2θ setup and Cu Kα radiation at 45 kV and 30 mA. Angles from 5 to 75° 2θ were scanned with a step size of 0.02° 2θ and 1s per step. ConvX software was used for file conversion, mineral identification was performed using DiffracPlus (EVA).

Raman spectroscopy

Raman (micro)spectroscopy was carried out using a custom made Raman spectrometer with an Argon ion laser tuned to 514 nm for excitation. The incident and scattered laser light is coupled in and out of an inverted Olympus IX71 microscope, equipped with a 20x air objective (Olympus, Numerical Aperture (NA)=0.75) or a 40x air UV objective (Thorlabs, NA=0.5). A motorized XYZ stage (Märzhäuser Wetzlar) in combination with a UV sensitive CCD camera allowed precise positioning of the samples. After the microscope, the light is dispersed using a spectrometer consisting of three stages (TriVista,

Princeton Instruments, purchased via S-and-I GmbH, Warstein, Germany) in subtractive dispersion mode. This allows recording of a broad spectrum while achieving good spectral resolution. The final readout of the optical spectrum is performed by a liquid nitrogen-cooled CCD camera. Data acquisition is handled by a personal computer running the software 'Vista Control' from S-and-I GmbH. For these measurements the power was set to 30 mW (514 nm) in the visible spectral range (5.5 mW in the deep UV, 244 nm). Integration times were 60 s long. To perform the analysis the mounted, polished sections were placed under the microscope, to select the analysis area.

ns-MC-LA-ICP-MS

Lead and strontium isotope analysis was performed by ns-LA-MC-ICP-MS, using an Analyte G2 193 nm ArF* excimer-based laser ablation system (Teledyne CETAC Technologies, Omaha, NE, USA) at the University of Ghent (Belgium). Glasses were analysed in line scan mode, ablating straight lines of 1 mm at 13 $\mu m \cdot s^{-1}$ translational speed, using masked beams of 30-130 µm diameter, 40 Hz frequency, and 4.05 $J \cdot cm^{-2}$ pulse energy.

Sr and Pb ion signals were measured using a Neptune MC-ICP-MS, operated with a constant flow of 3% HNO_3 at 100 $\mu l \cdot min^{-1}$. This approach was also used to introduce a Tl internal standard solution (150 $\mu g \cdot l^{-1}$) into the LA aerosol transport line while measuring Pb isotope ratios.

Sr isotopes were measured in medium resolution and mass bias correction was achieved using the exponential law and the samples' $^{88}Sr/^{86}Sr$ ratios as internal standard. Lead isotope ratios were measured in low resolution and mass bias correction was achieved through the revised Russell's law using Tl as internal standard and Corning glass D as external standard (Van Ham-Meert et al., 2018).

Boron isotopic analysis was carried out using LA-MC-ICP-MS (Goethe University Frankfurt, Germany) with the method adopted from Devulder et al. (2015). Analysis consists of 20s gas background and 25s sample ablation, with static spots of 213 µm, 10 Hz repetition rate, 2.5 $J \cdot cm^{-2}$ energy density, appropriate bracketing standards were also measured (NIST 610, B6) applying identical ablation conditions (spot size, laser fluence etc.). The raw measurement data was corrected for biases induced by the background and mass discrimination. Differences in isotopic composition of boron are expressed as the relative difference in isotopic ratio between the unknown sample and the isotopic reference material NIST 951 boric acid (NIST, MD, USA, $(^{11}B/^{10}B)_{NIST\ SRM951}$ = 4.0436 ± 0.0027 (2σ), Catanzaro et al. 1970).

3 Results

3.1 Elemental composition

The elemental composition of samples Sa-01 to Sa-03 are shown by colour in Table 2, with y and bl respectively denoting yellow and black.

First, reduced base glass compositions (indicated by *) are considered (Table 3). These are determined as the total amount of the oxides Na_2O, MgO, Al_2O_3, SiO_2, P_2O_5, K_2O, CaO and Fe_2O_3 normalised to 100 wt% (similar approach to Brill, 1999; Panighello et al., 2012). It represents the base glass composition without any (de)colouring and/or opacifying agents. The concentration of iron oxide can be influenced by the addition of (de)colouring and opacifying agents to the glass batch (Brill, 1999). Therefore the iron concentration in the "base glass" does not necessarily reflect the iron content in the silica and/or flux source.

The reduced compositions of the black and yellow glasses are different (Table 3). The reduced composition of the black glass yields approximately 12 wt% less SiO_2, the absolute SiO_2 concentration is also higher in Sa-01bl and Sa-02bl (Table 2). Assuming the base glass used for both glass colours has

the same composition, there needs to be a second independent silica source for the yellow glass, the colouring agent.

The second important difference between the yellow and black glass is the higher iron concentration in the black glass, due to the addition of an iron compound to obtain the dark colour.

Potash (K_2O) and magnesia (MgO) concentrations above 1.5 wt% are typical of glasses fluxed with plant ash (Sayre and Smith, 1961). Here, K_2O* is > 2.0 wt% for all samples, whereas MgO* is below 1.5 wt % (Table 3 and Fig. 2). Based on these numbers, it is not possible to classify the samples unambiguously as plant ash or natron glass. Nevertheless, the lime concentrations below 3 wt% indicate that plant ash is an unlikely flux for these glasses. The low lime levels in the beads are positively associated with strontium concentration, with mean values of 2.5 wt% and 245 ppm respectively. The $^{87}Sr/^{86}Sr$ ratio of the beads varies around 0.71733 (Table 4), which is much more radiogenic than most ancient glass analysed, pointing towards a silica raw material originating from a granitic source rock (Brems et al. 2013), provided that the Sr source in the glass beads is the silica raw material and not a plant ash flux.

Figure 2: Potash versus magnesia for the samples from Sardis (reduced concentrations for the yellow and black parts of the samples)

Trace element analysis reveals elevated concentrations for the elements titanium, vanadium, chromium and arsenic. The strong correlation between titanium and niobium points to the presence of rutile in the raw material used, while the significant amounts of potash positively correlated with rubidium and barium can be explained by the occurrence of alkali feldspar (Brems and Degryse, 2014). The silica source must also have contained minerals such as zircon ($ZrSiO_4$) indicated by the presence of zirconium and hafnium in the glass, monazite $(Ce,La,Y,Th)PO_4$ providing lanthanum and thorium, and garnet $(Mg,Fe,Mn,Ca)_3(Al,Fe,Cr)_2Si_3O_{12}$ causing the presence of yttrium in the beads (Brems and Degryse, 2014). This indicates the use of a sand source with a significant non-quartz mineral content. The presence of these minerals is also confirmed by the enriched Rare Earth Element (REE) pattern of the glass beads. The values normalised to the Earth's Continental Crust composition (according to Wedepohl, 1995) increase steeply from lanthanum to lutetium with the occurrence of a negative europium anomaly (Fig. 3). Such anomaly is typical for granitic rocks of the Earth's upper Continental Crust (Wedepohl and Simon, 2010). The yellow and black glasses follow the same pattern, although the black glasses have a higher absolute concentration in REEs. The similarity in pattern indicates the sand source of the base glass used for the production of the yellow and black colours is likely homologues, while the difference in absolute concentration is due to the addition of Pb and Sn in high amounts to the yellow glass.

Figure 3: Line plot of the average REE concentrations of the analysed samples normalized to abundances in the Earth's Continental Crust (Wedepohl, 1995) together with REE patterns for Turkish high-boron high-alumina glasses (Dussubieux et al. 2010) and sands near Sardis (Kealhofer et al. 2013).

Samples Sa-01 to Sa-03 have an exceptionally high alumina boron and lithium content, in excess of 4.5 wt% 2500 ppm, and 100 ppm respectively (Table 2), with $\delta^{11}B$ values of around +0.3‰ (Table 4).

Elevated amounts of boron were most likely introduced with the flux, as suggested by the strong correlation of boron with several alkali and alkaline earth metals such as lithium, potassium, rubidium and caesium. Alumina likely entered the glass through the silica raw material used. The high

concentrations of alumina, the high $^{87}Sr/^{86}Sr$ ratio and the REE pattern all point towards a granitic source for this silica.

3.2 Pigment identification

The dark colour of the black glass is caused by high iron concentrations, while the opaque yellow glass shows high lead and tin contents, with average values of 21.1 and 2.4 wt% Pb and Sn, respectively, also associated with elevated contents of copper, arsenic, silver, antimony and bismuth (Table 2). The yellow part of sample Sa-04 was subjected to XRD analysis. On Fig. 4, apart from the amorphous background indicative of the glass phase present, 5 peaks can be distinguished respectively at 2θ= 14.6°, 29.1°, 33.6°, 48.3°, and 57.4°. These peaks are in close agreement with those recorded by Bagdzevičiene et al. (2011) for lead-tin yellow type II pigment (2θ= 29°, 33.5°, 48° and 57°).

Figure 4: Diffraction pattern of yellow sample Sa-04, the diffraction peaks are indicated together with their d-value. This pattern corresponds to $PbSn_{1-x}Si_xO_3$

Analysis of yellow parts of beads Sa-01 (2 measurements) and Sa-02 (1 measurement) was achieved non-destructively using Raman spectroscopy. The Raman spectra are shown in Fig. 5. The main peaks and bands at 64, 137, 193, 327 and 448 cm^{-1}, with a shoulders around 79 and 95 cm^{-1} correspond well to those characteristic for lead-tin yellow type II (Bagdzevičiene et al., 2011). A small amount of yellow type I is also resolved with characteristicpeaks at 196 and 455 cm^{-1} well resolved while others overlap with those of lead-tin yellow type II. The yellow opacifying agent is therefore consistent with being mainly type II, with a minor presence of type I.

Figure 5: ***Raman shift for samples Sa-01 (2 different spots) and Sa-02,the chemical compounds corresponding to different peaks are also given.***

Lead isotopic analysis on the yellow parts of the glass beads yields results which are not in agreement with each other (Table 4). The three measurement points were compared to the OxaLid data-base (Stos-Gale et al., 2009). Samples do not fit any of the ore deposits from the data-base. The high variability in lead isotope signature reflects the use of more than one lead ore source for the production of the opacifying agent.

3.3 Microstructure

Backscattered images (BSE) (Fig. 6) of the yellow glass reveal an inhomogeneous distribution of euhedral and anhedral crystals of lead stannate in the glass matrix. This distribution is consistent with the addition of the already formed pigment to the glassy matrix (Rooksby et al., 1964).

Figure 6: BSE images, sample Sa-02 euhedral lead stannate crystals (scale bar represents 10 µm).

4 Discussion

From the different analytical approaches followed, it can be concluded that the glass beads studied are extraordinary in their composition and recipe. Only a limited number of samples were studied, reflecting the low number of glass fragments available, but glass from the eight to seventh century BCE with such high alumina content and this particular opacifier/colourant have not (yet) been found outside Sardis. The scarcity of this glass could be explained by it being a short-lived and/or fast-evolving, most likely experimental production phase.

4.1 Sand source

Glass with alumina concentrations > 4 wt% and boron concentrations > 500 ppm is rare in ancient times (Rehren et al., 2015; Schibille, 2011). Dussubieux et al. (2010) reported the composition of artefacts from Sardis dating to the twelfth to fourteenth centuries CE, classified as m-Na-Al 5, closely resembling the data for samples Sa-01, Sa-02, and Sa-03. Furthermore, the REE patterns of both glass assemblages almost perfectly match (Fig. 7). This could suggest the use of similar raw materials in the production of these glasses, despite the considerable chronological gap. To date, no primary glassmaking centres for this kind of glass have been discovered. For the "High Alumina Glasses" from Sardis analysed by Brill (2012), "black sands" rich in alumina and containing monazite have been suggested as a raw material. This glass has a radiogenic strontium isotope signature ($^{87}Sr/^{86}Sr$ = 0.715-0.717), but contains more lime than the Iron Age glass from Sardis.

The silica source used for producing the beads found at Sardis has a significant non-quartz mineral content, with a REE pattern differing from any known glass group (Wedepohl et al. 2011). Kealhofer et al. (2013) report the analysis of fine white sand from a quarry 9 km west of Sardis. Although no alumina concentrations are available and the match between the composition of this sand and the studied glass is not perfect, similarities in REE pattern (Fig. 7) and trace element contents could be indications of the use of a similar raw material for the production of the Sardis glass beads. Such sediment would also explain the strontium isotopic composition of the glass, as the bedrock contains schist and granite-derived gneiss (Kealhofer et al., 2013, and references therein), causing a more radiogenic strontium isotopic signature of the sand weathered from it (Vengosh et al., 2002). It needs to be stated that the use of this silica source near Sardis would imply a local production for the glass studied here as well as the glass published by Dussubieux et al. (2010) (Fig. 3), a suggestion not corroborated by archaeological excavation.

4.2 Flux source

As the boron content in the glass beads is correlated with several alkali and alkaline earth metals, it is likely that boron entered the glass with the flux material (Schibille, 2011). There are two possible types of flux which would account for the high boron concentrations, whilst also providing the alkalis.

The first possibility is the use of polyphase evaporitic lake deposits. There are evaporate deposits related to the major borate deposits in western Anatolia (Schibille, 2011). The principal boron minerals found there are colemanite ($CaB_3O_4(OH)_3.H_20$), ulexite ($NaCaB_5O_6(OH)_6.5H_2O$) and borax ($Na_2B_4O_5(OH)_4.8H_2O$), formed in lacustrine settings and hosted in Miocene calc-alkaline volcanoclastic deposits (Palmer and Helvaci, 1997). Evaporation in these non-marine lakes produces alkaline brines characterized by the presence of (bi)carbonates, sulphates, chlorides and borates (Helvaci et al., 2004; Garcia-Veigas and Helvaci, 2013). Consistent with the analysed glass samples, considerable – although variable – amounts of lithium and arsenic are detected in these borate deposits, but the detected sodium levels are low (Helvaci et al., 2004; Lin et al., 2011; Helvaci, 2015). Borate deposits in western Anatolia show relatively low $\delta^{11}B$ values with a wide range from -1.6 to -25.3‰ (Palmer and Helvaci, 1995; 1997), primarily controlled by their mineralogy. Since important mineralogical differences exist between borate districts in western Anatolia (Garcia-Veigas and Helvaci, 2013), it is possible that the slightly positive boron signatures of the glass beads are derived from this kind of deposits. In addition, trona deposits north of Beypazari, located 100 km west of Ankara, at present exploited for the production of soda ash and its derivatives, are other alkali sources potentially used during the Iron Age and at later times (Dardeniz, 2015).

Alternatively, flux can be produced from soda-rich salts by evaporating water from hot springs to dryness. The resulting sodium (bi)carbonate crystals could have been added to the glass batch during the manufacturing process of the glass studied here (Tite et al., 2016). Vengosh et al. (2002)

investigated the chemical and isotopic composition of several thermal waters from the Menderes Massif and distinguished four major types of source water. The Na-HCO_3 group, of interest in view of the flux used in the high-boron glasses, is characterized by elevated boron levels with a boron isotopic composition between -2.3 and +1.8‰. The matching ratios in Na/K, Na/Mg, K/Mg and Na/B between the high boron glasses and the hot spring waters of the Na-HCO_3 type in the vicinity of Sardis (Table 5; Vengosh et al., 2002) could indicate the use of local hot springs. Furthermore, this kind of flux would provide a convenient explanation for the elevated potash versus magnesia concentrations detected in the glass samples, seen from the overlap in K/Mg ratios (Table 5). This second option thus not only complies more satisfactorily with the boron isotopic signature of the samples considered here, but would also explain the potash concentration and the potash to magnesia ratio found in the glasses. The Na-HCO_3 springs have also been suggested as the source of flux for medieval high Al-B glasses (up to 3000 ppm B) from Ḥiṣn al-Tīnāt (Swan et al. 2018). A clear direct link cannot be made for materials that are nearly two millennia apart, but the possibility of a continued production of this glass type in the region over a prolonged period is an intriguing one which warrants further study of glass assemblages in that region.

Recently, more analytical data for late Bronze Age high-boron glass beads from Jordan and Hasanlu have been published. These are lower in B content (around 1500 ppm) than the beads in this study, and it was suggested that the flux used was mineral soda from Northwestern Iran (Dussubieux et al. 2018). Additionally, Bronze Age beads with high B, Al and Li (though all with lower contents than the beads from Sardis) were found in Central Europe (Mildner et al. 2018), for which it was suggested they could have a Western Anatolian origin. All these finds provide further clues for the existence of mineral soda glass making, characterised by elevated boron concentrations, different from the commonly known mineral soda glass.

It seems this glass tradition with elevated B, Al and/or Li, of which the glass from Sardis is an early example, continues or is reused, from the first century CE onwards in Pergamon and more generally in Western Anatolia during the Byzantine period (Rehren et al. 2015, Swan et al. 2018). These later glasses are often dark blue but coloured with cobalt, whereas the black glass from Sardis is coloured by iron (similar to the Romanian glass) (Bugoi et al. 2016). The glass from Sardis is richer in boron and alumina than HLiBAl glass, and poorer in CaO and lithium, whereas it contains levels of alumina similar to the HBAl glass, but with more elevated boron and lithium concentrations.

4.3 Lead stannate

The yellow glass trails on the black beads are formed by lead-tin yellow type II, as shown by XRD and Raman spectroscopy. The use of lead stannate rather than lead antimonate for producing this yellow opaque colour is exceptional, and could point to a local innovation. Since the elevated Sn and Pb concentrations are associated with bismuth, silver, antimony, arsenic and copper, in concentrations higher than expected for individual ores a metallurgical source for this material is suggested.

Lead was probably common in Lydian Sardis and could have come from multiple sources reflecting the varied interests and regions controlled by the Lydians. This observation is in line with the limited lead isotopic data available on other materials from Sardis, reflecting the use of many different ore sources (Lydia, Brill and Shields, 1972; Brill and Wampler, 1967; Lavrion, Eiseman, 1980).

The preparation of lead-stannate apart from the glass and in the presence of silica is in line with finds from early medieval Europe (Heck et al. 2003). Heck et al. (2003) were unsure whether the elevated silica concentrations would be present in the bulk of the pigment (they only studied a residue layer inside a crucible), but the finds in this study prove they are also found in the bulk of the pigment.

5. Conclusion

The eighth to seventh centuries BCE constitute a vital interval in the complex history of glass manufacture. It is a period of transition from the use of plant ash to mineral soda as flux in glass technology. This study presents new findings on black and yellow glass beads from Sardis. The base glass composition shows that the silica source used is likely granite derived, with high alumina concentrations, while the alkali source is consistent with the use of a mineral soda rich in boron. Such silica source is available around Sardis in the form of white sands described by Kealhofer et al. (2013) and black sands described by Brill (2012). Furthermore, the region around Sardis boasts many hot springs where natron could be won from evaporating water. This source of natron could explain the high potassium and low magnesium and calcium concentrations in the glass, which are also observed in later glass from the area. All of this suggests a local, experimental, primary glass production in Sardis during the Lydian period. The opacifying agent used is lead-tin yellow type II, predating the earliest known occurrence of this type of colourant by at least four centuries.

The glass samples scrutinised here are extraordinary experimental artefacts, of which only a limited quantity survived. As such they represent a unique snapshot in the development of glass technology in Anatolia during the Middle Iron Age. They seem, however, to be part of a larger corpus of high aluminium and boron mineral soda glasses produced in the Bronze Age as evidenced by other recent finds. It is hoped these new finds will contribute to the current discussion on high alumina and boron glass in Anatolia and will shed further light on this particular glass making tradition.

References

Arletti R, Rivi, L, Ferrari D, Vezzalini G (2011) The Mediterranean Group II: Analyses of vessels from Etruscan contexts in northern Italy. *Journal of Archaeological Science* 38: 2094-2100.

Bagdzevičienė J, Niaura G, Garškaitė E, Senvaitienė J, Lukšėnienė J, Tautkus, S (2011) Spectroscopic analysis of lead tin yellow pigment in medieval necklace beads from Kernave-Kriveikiškes cemetery in Lithuania. *Chemija* 22: 216-222.

Brems D, Ganio M, Latruwe K, Balcaen L, Carremans M, Gimeno D, Silvestry A. Vanhaecke F, Munchez P, Degryse P (2013) Isotopes on the beach, part 1: Strontium isotope ratios as a provenance indicator for lime raw materials used in Roman glass-making. *Archaeometry* 55: 214-234.

Brems D, Degryse P (2014) Trace element analysis in provenancing Roman glass-making. *Archaeometry* 56: 116-136.

Brill RH, Wampler JM (1967) Isotope studies of Ancient Lead. *American Journal of Archaeology* 71: 63-77.

Brill RH, Shields WR (1972) Lead isotopes in Ancient Coins. *Methods of Chemical and Metallurgical Investigation of Ancient Coinage* 8: 272-303.

Brill RH (1999) *Chemical Analyses of Early Glasses* (Corning Museum of Glass, Corning, New York).

Brill RH (2012) Chemical analyses of early glasses in *The Years 2000-2011, Reports, and Essays, vol. 3.* (Corning Museum of Glass, Corning, New York).

Bugoi, R., Poll, I., Manucu-Adamesteanu, G., Calligaro, T., Pichon, L., & Pacheco, C. (2016). PIXE–PIGE analyses of Byzantine glass bracelets (10th–13th centuries AD) from Isaccea, Romania. *Journal of*

Radioanalytical and Nuclear Chemistry, 307: 1021-1036. 10.1007/s10967-015-4240-0

Cahill ND (2010a) *Lidyalılar ve Dünyaları / The Lydians And Their World*. Istanbul: Yapı Kredi Yayınları; available online at http://sardisexpedition.org/en/publications/latw.

Cahill ND, Hari J, Önay B, Dokumacı E (forthcoming), "Depletion Gilding of Lydian Electrum Coins and the Sources of Lydian Gold." in P. van Alfen, U. Wartenberg, W. Fischer-Bossert, H. Gitler, and K. Konuk, eds. *White Gold: Studies in Early Electrum Coinage*. New York and Jerusalem: American Numismatic Society and Israel Museum.

Catanzaro EJ, Champion CE, Garner EL, Marinenko G, Sappenfield KM, Shields WR (1970) Boric acid; isotopic, and assay standard reference materials. *US National Bureau of Standards, Special Publication 260-17*: 70 pp.

Conte S, Arletti R, Mermati F, Gratuze B (2016a) Unravelling the Iron Age glass trade in southern Italy: The first trace-element analyses. *European Journal of Mineralogy* 28: 409-433.

Conte S, Arletti R, Henderson J, Degryse P, Blomme A (2016b) Different glassmaking technologies in the production of Iron Age black glass from Italy and Slovakia. *Archaeological and Anthropological Sciences* 10:503-521 doi.org/10.1007/s12520-016-0366-4.

Dardeniz G (2015) Was ancient Egypt the only supplier of natron? New research reveals major Anatolian deposits. *Anatolica* 41: 191-202.

Devulder V, Gerdes A, Vanhaecke F, Degryse P (2015) Validation of the determination of the B isotopic composition in Roman glasses with laser ablation multi-collector inductively coupled plasma-mass spectrometry. *Spectrochimica Acta - Part B Atomic Spectroscopy* 105: 116-120.

Dickinson O (2006) *The Aegean from Bronze Age to Iron Age – Continuity and Change between the Twelfth and Eighth Centuries BC* (Routledge, London), 298 pp.

Drew R (1993) *The end of the Bronze Age – Changes in warfare and the catastrophe ca. 1200 B.C.* (Princeton University Press, Princeton, New Jersey), 264 pp.

Dussubieux L, Gratuze B, Blet-Lemarquand M (2010) Mineral soda alumina glass: occurrence and meaning. *Journal of Archaeological Science* 37: 1646-1655.

Dussubieux, L., Schmidt, K., Rowan, Y. M., Wasse, A. M. R., & Rollefson, G. O. (2018). Notes: Two glass beads from Wisad pools in the Jordanian black desert. *Journal of Glass Studies, 60*, 303-306

Eiseman CJ (1980) Greek Lead, Ingots from a Shipwreck Raise Questions about Metal Trade in Classical Times. *Expedition* 22: 41-47.

Ganio M, Boyen S, Brems D, Scott R, Foy D, Latruwe K, Molin G, Silvestri A, Vanhaecke F, Degryse P (2012) Trade routes across the Mediterranean: a Sr/Nd isotopic investigation on Roman colourless glass. *Glass Technology: European Journal of Glass Science and Technology A* 53: 217–24.

García-Veigas J, Helvacı C (2013) Mineralogy and sedimentology of the Miocene Göcenoluk borate deposit, Kırka district, western Anatolia, Turkey. *Sedimentary Geology* 290: 85-96.

Gratuze B, Blet-Lemarquand M, Barrandon J (2001) Mass spectrometry with laser sampling: A new tool to characterize archaeological materials. *Journal of Radioanalytical and Nuclear Chemistry* 247: 645-656.

Gratuze B, Picon M (2005) Utilisation par l'industrie verrière des sels d'aluns des oasis égyptiennes au début du premier millénaire avant notre ère. *L'Alun de Méditerranée*, eds Borgard P, Brun JP, Picon M (Collection du Centre Jean Bérard 23, Naples), pp 269-276.

Gratuze B (2009) Les premier verres au natron retrouvés en Europe Occidentale: composition chimique et chrono-typologie. *Annales du 17e Congrès de l'Association Internationale pour l'Histoire du Verre (2006)* eds Janssen K, Degryse P, Cosyns P, Caen J, Van 't Dack L (Antwerp), pp 8-14.

Hanfmann GMA, Mierse WE (1983) *Sardis from Prehistoric to Roman Times. Results of the Archaeological Exploration of Sardis 1958-1975* (Harvard University Press, Cambridge, Massachussetts), 466 pp.

Hartmann G, Kappel I, Grote K, Arndt B (1997) Chemistry and technology of prehistoric glass from lower Saxony and Hesse. *J. Archaeol. Sci*. 24: 547-559.

Heck, M., Rehren, Th., & Hoffmann, P. (2003) The production of lead-tin yellow at Merovingian Schleitheim (Switzerland). *Archaeometry, 45*: 33-44.

Helvaci C, Mordogan H, Çolak M, Gündogan I (2004) Presence and distribution of lithium in borate deposits and some recent lake waters of West-Central Turkey. *International Geology Review* 46: 177-190.

Helvaci C (2015) Review of the occurrence of two new minerals in the Emet borate deposit, Turkey: emetite, $Ca_7Na_3K(SO_4)_9$, and fontarnauite, $Na_2Sr(SO_4)[B_5O_8(OH)](H_2O)_2$. *Bulletin of the Mineral Research and Exploration* 151: 269-283.

Henderson J (1988) Electron probe microanalysis of mixed-alkali glass. *Archaeometry* 30:77-91.

Henderson J (2013) *Ancient Glass: An Interdisciplinary Exploration* (Cambridge University Press, Cambridge, UK): doi.org/10.1017/CBO9781139021883.

Karydis ND (2012) A monument of early Byzantine Sardis: architectural analysis and graphic reconstruction of Building D. *Anatolian Studies* 62: 115-139.

Kealhofer L, Grave P, Marsh B (2013) Scaling ceramic provenience at Lydian Sardis, Western Turkey. *Journal of Archaeological Science* 40: 1918-1934.

Lin J, Pan Y, Chen, N, Mao M, Li R, Feng R (2011) Arsenic incorporation in colemanite from borate deposits: data from ICP-MS, µ-SXRF, XAFS and EPR analyses. *The Canadian Mineralogist* 49: 809-822.

Mildner, S., Schüssler, U., Falkenstein, F., & Brätz, H. Bronzezeitliches "High-magnesium glass" in Mitteleuropa- Lithium und Bor als Indizien für eine mögliche Herkunft aus Westanatolien. *Archaeometrie Und Dankmalpflege,* Hamburg. pp. 132-135.

Neri, E., Schibille, N., Pellegrino, M., & Nuzzo, D. (2019). A Byzantine connection: Eastern Mediterranean glasses in Medieval Bari. *Journal of Cultural Heritage,* doi:10.1016/j.culher.2018.11.009

Palmer MR, Helvaci C (1995) The boron isotope geochemistry of the Kirka borate deposit, western Turkey. *Geochimica et Cosmochimica Acta* 59: 3599-3605.

Palmer MR, Helvaci C (1997) The boron isotope geochemistry of the neogene borate deposits of western Turkey. *Geochimica et Cosmochimica Acta* 61: 3161-3169.

Panighello S, Orsega EF, van Elteren JT, Šelih VS (2012) Analysis of polychrome Iron Age glass vessels from Mediterranean I, II and III groups by LA-ICP-MS. *Journal of Archaeological Science* 39: 2945-2955.

Pearce NJG, Perkins WT, Westgate JA, Gorton MP, Jackson SE, Neal CR, Chenery SP (1997) A compilation of new and published major and trace element data for NIST SRM 610 and NIST SRM 612 glass reference materials. *The Journal of Geostandards and Geoanalysis* 21: 115-144.

Purowski T, Dzierzanowski P, Bulska E, Wagner B, Nowak A (2012) A study of glass beads from the Hallstatt C-D from southwestern Poland: implications for Glass technology and provenance. *Archaeometry* 54: 144-166.

Reade W, Freestone IC, Simpson SJ (2006). Innovation or continuity? Early first millennium BCE glass in the Near East: the cobalt blue glasses from Assyrian Nimrud. *Annales du 16^{e} Congrès de l'Association International de l'Histoire du Verre*, ed Cool H. (J.W. Arrowsmith, Bristol, Nottingham) pp 23-27.

Reade W, Freestone IC, Bourke S (2009) Innovation and continuity in Bronze and Iron Age glass from Pella in Jordan. In *Annales du 17^{e} Congrès de l'Association Internationale de l'Histoire du Verre (2006)*, eds Janssens K, Degryse P, Cosyns P, Caen J, Van't Dack L (Antwerp) pp 47-54.

Rehren, Th., Connolly P, Schibille N, Schwarzer H (2015) Changes in glass consumption in Pergamon (Turkey) from Hellenistic to late Byzantine and Islamic times. *Journal of Archaeological Science* 55: 266-279.

Rehren, Th., Freestone, I. C. (2015). Ancient glass: From kaleidoscope to crystal ball. *Journal of Archaeological Science, 56*: 233-241. dx.doi.org/10.1016/j.jas.2015.02.021

Rooksby HP (1964) A yellow cubic lead tin oxide opacifier in ancient glasses. *Physics and Chemistry of Glass* 5: 20-25.

Roosevelt CH (2006) Tumulus Survey and Museum Research in Lydia , Western Turkey : Determining Lydian- and Persian-Period Settlement Patterns. *Journal of Field Archaeology* 31 (1): 61–76.

Sayre EV, Smith RW (1961) Compositional categories of ancient glass. *Science* 133: 1824-1826.

Schibille N (2011) Late byzantine mineral soda high alumina glasses from asia minor: A new primary glass production group. *PLoS ONE* 6: https://doi.org/10.1371/journal.pone.0018970

Schlick-Nolte B, Werthmann R (2003) Glass vessels from the burial of Nesikhons. *Journal of Glass Studies* 45: 11-34.

Sekedat BM (2016) X-Ray Fluorescence and Stable Isotope Analysis of Marble in Central Lydia, Western Turkey. *Oxford Journal of Archaeology* 35: 369-388.

Shortland AJ, Eremin K (2006) The analysis of second millennium glass from Egypt and Mesopotamia, Part 1: New WDS analyses. A*rchaeometry* 48: 581-603.

Stos-Gale Z, Gale NH (2009) Metal provenancing using isotopes and the Oxford archaeological lead isotope database (OXALID). *Archaeological and Anthropological Science* 1(3): 195-213.

Swan, C. M., Rehren, Th., Dussubieux, L., & Eger, A. A. (2018). High-boron and high-alumina middle byzantine (10th–12th century CE) glass bracelets: A Western Anatolian glass industry. *Archaeometry, 60*(2), 207-232

Tite M, Pradell T, Shortland A (2008) Discovery and use of tin-based opacifiers in glasses, enamels and glazes from the late iron age onwards: a reassessment*. Archaeometry* 50: 67-84.

van Elteren JT, Tennent NH, Šelih VS (2009) Multi-element quantification of ancient/historic glasses by laser ablation inductively coupled plasma mass spectrometry using sum normalization calibration. *Analytica Chimica Acta* 644: 1-9.

Van Ham-Meert A, Chernonozhkin S, Van Malderen SJM, Van Acker T, Vanhaecke F, Degryse P (2018) Assessment of nanosecond Laser Ablation Multi-collector - Inductively Coupled Plasma - Mass Spectrometry for Pb and Sr isotopic analysis of archaeological glass – mass bias correction strategies and results for Corning glass Reference materials. *Geostandards and Geoanalytical Research* 42(2):223-238 DOI 10.1111/ggr.12202

Vicenzi EP, Eggins S, Logan, A, Wysoczanski R (2002) Microbeam Characterization of Corning Archeological Reference Glasses: New Additions to the Smithsonian Microbeam Standard Collection. *Journal of Research of the National Institute of Standards and Technology* 107: 719-727.

Fig. 1. Beads from Lydian Sardis, Sa-01 (a), Sa-02 (b), Sa-03 (c).

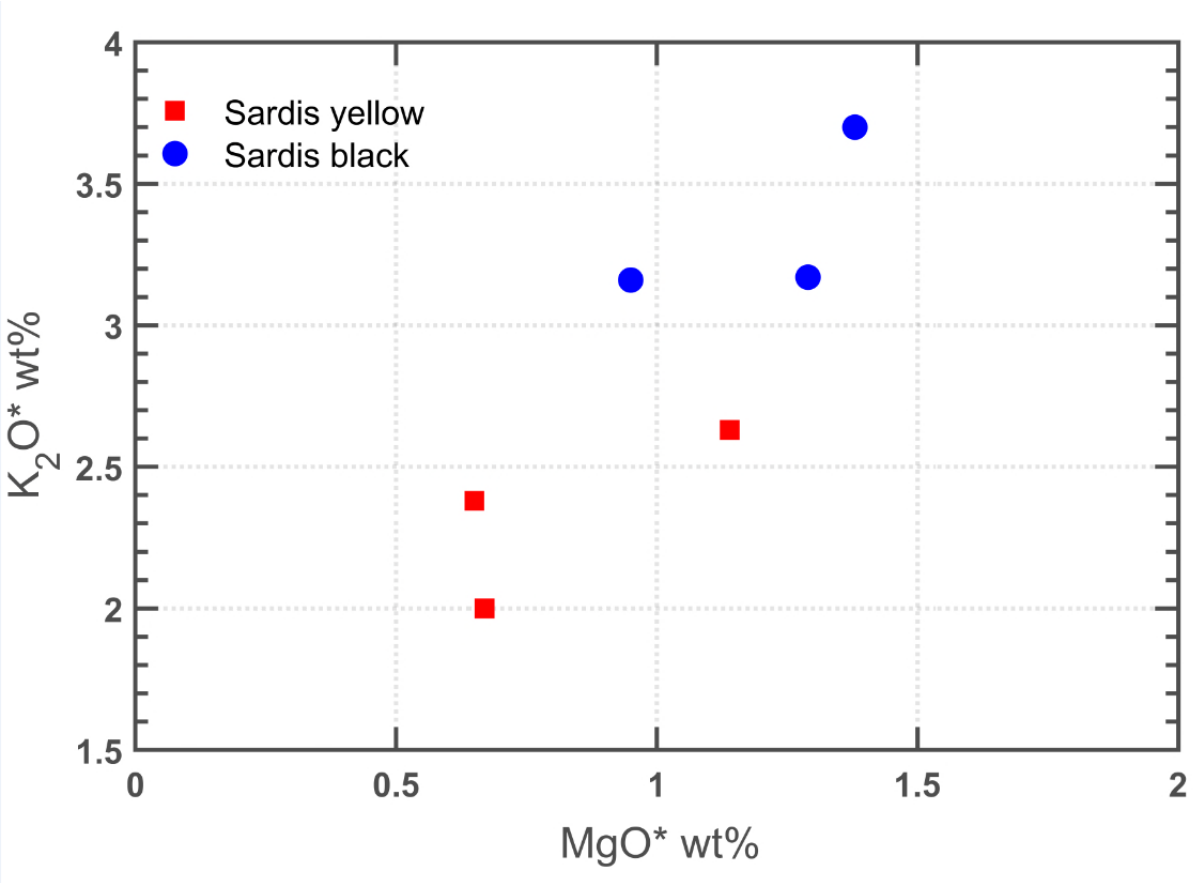

Fig. 2. Potash versus magnesia for the samples from Sardis (reduced concentrations for the yellow and black parts of the samples).

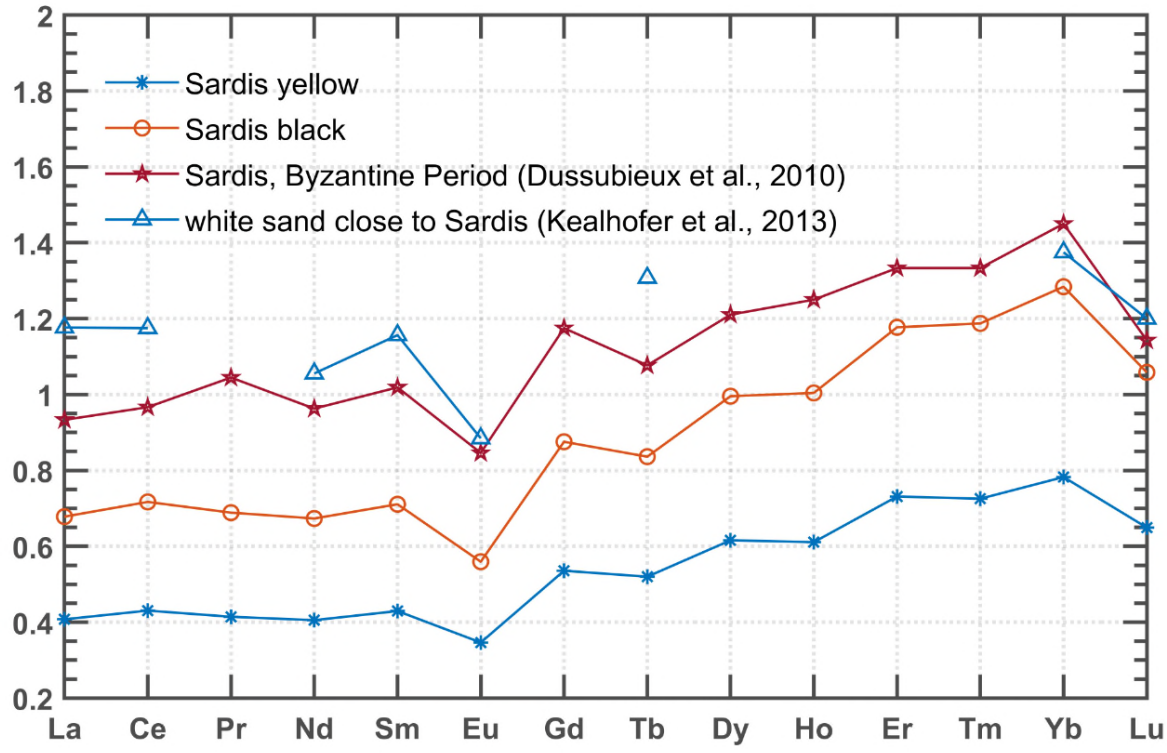

Fig. 3. Line plot of the average REE concentrations of the analysed samples normalised to abundances in the Earth's Continental Crust (Wedepohl, 1995) together with REE patterns for Turkish high-boron high-alumina glasses (Dussubieux et al., 2010) and sands near Sardis (Kealhofer et al., 2013).

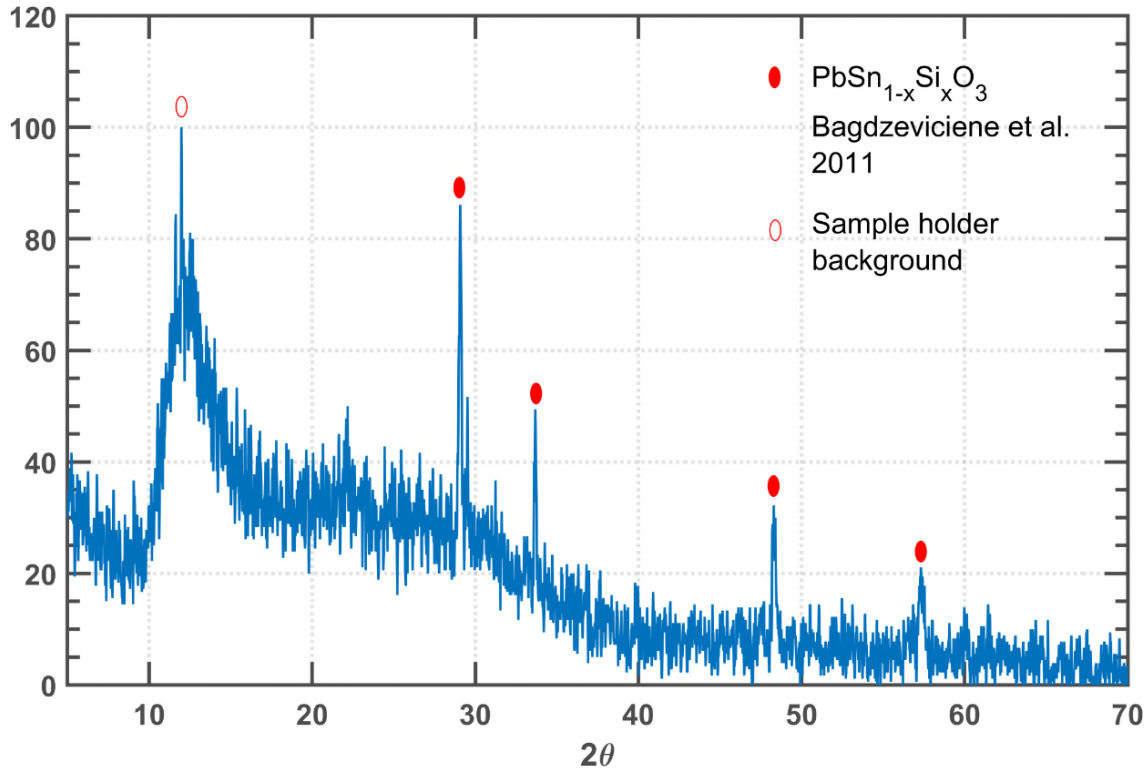

Fig. 4. Diffraction pattern of yellow sample Sa-04, the diffraction peaks are indicated together with their d-value. This pattern corresponds to $PbSn_{1-x}Si_xO_3$.

Fig. 5. Raman shift for samples Sa-01 (2 different spots) and Sa-02, the chemical compounds corresponding to different peaks are also given.

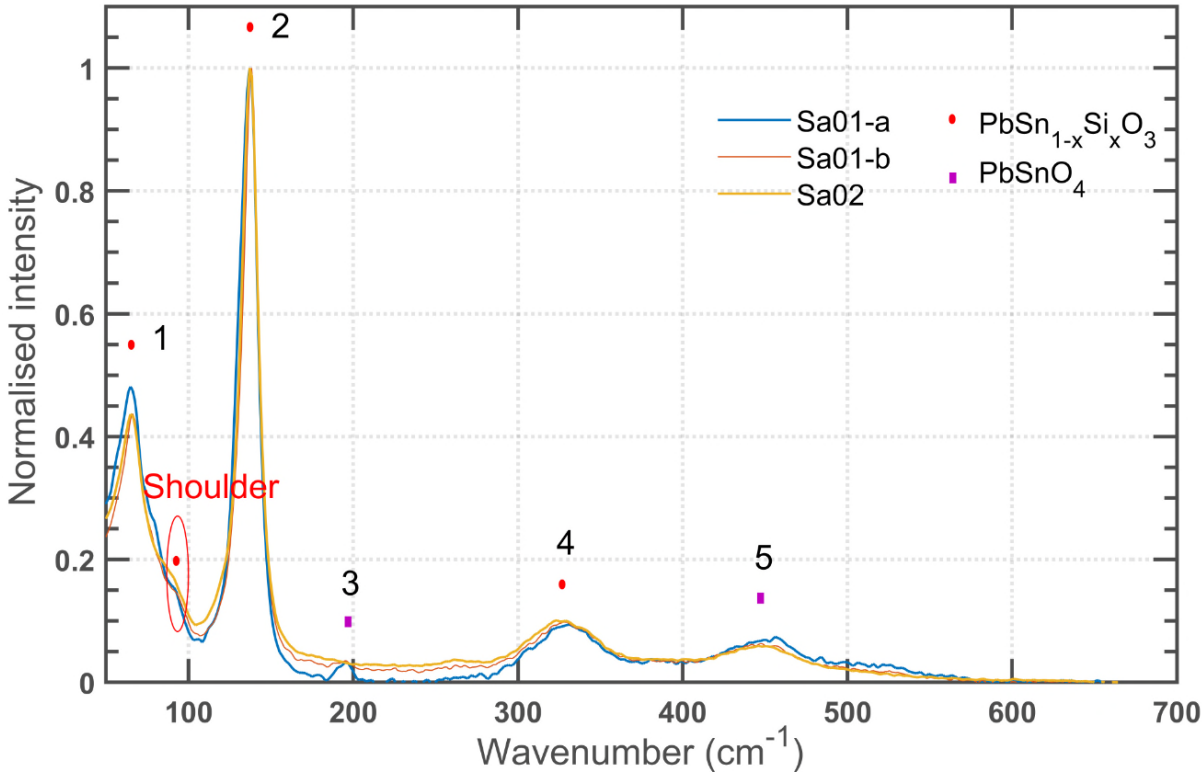

Fig. 5. Raman shift for samples Sa-01 (2 different spots) and Sa-02, the chemical compounds corresponding to different peaks are also given.

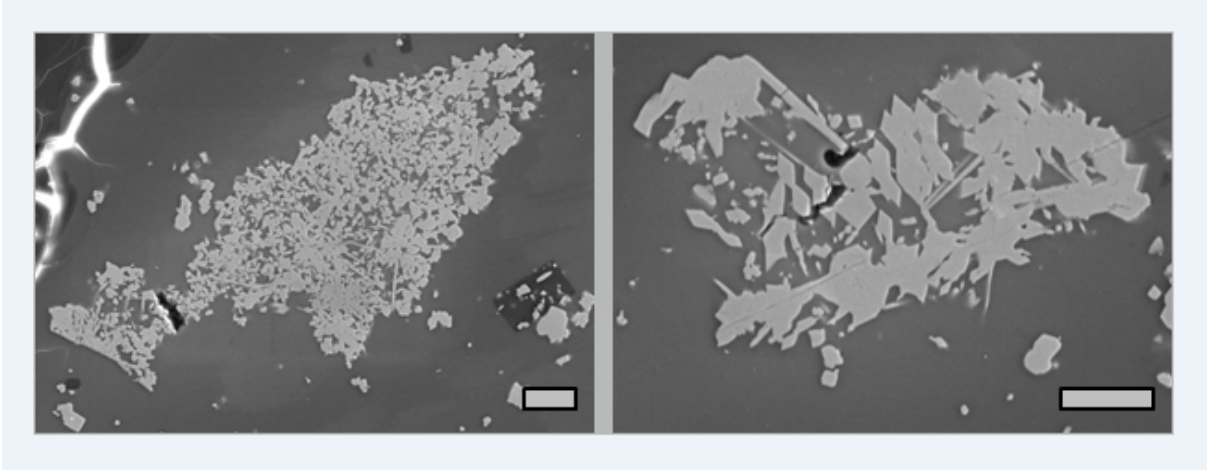

Fig. 6. BSE images, sample Sa-02 euhedral lead stannate crystals (scale bar represents 10 μm).

Table 1: Overview of samples, the type of performed analysis is given as well as numbers from the excavation site and date

		colour	performed analysis			field name	date	Object type / typology
			EPMA	Raman/XRD	LA-MC-ICP-MS			
Sa-01	a	yellow	x	Raman	Pb	Cat G08.001 12310	7th century BCE	Eye bead
	b	black	x		Sr & B			
Sa-02	a	yellow	x	Raman	Pb	Cat G09.005 12423	Late 8th to early 7th century BCE	Spherical eye bead
	b	black	x		Sr			
Sa-03	a	yellow	x		Pb	Cat G09.002 12407	Late 8th to early 7th century BCE	Spherical eye bead
	b	black	x		Sr & B			
Sa-04	a	yellow		XRD		G62.12.4523	~700 BCE	bead
	b	black						

Table 2: Elemental composition obtained by EPMA ([a]) or LA-ICP-MS ([b]), oxides are in wt% and elements in ppm, LOD are expressed in ppm. Y is the yellow part, bl the black part, n.d.: not detected, bdl: below detection limit.

Number	LOD	Corning B	Corning A	Sa-01y	Sa-01bl	Sa-02y	Sa-02bl	Sa-03y	Sa-03bl
Na_2O[a]	42	16.94		12.92	21.52	10.91	21.01	14.07	19.99
MgO[a]	45	1.04		0.81	1.25	0.45	1.32	0.53	0.92
Al_2O_3[a]	26	4.49		6.09	9.41	4.53	10.23	7.29	8.96
SiO_2[a]	44	61.7		45.72	54.00	45.95	53.70	54.12	52.95
P_2O_5[a]	43	0.87		0.15	0.20	0.11	0.27	0.13	0.21
SO_3[a]	17	0.35		0.09	0.18	n.d.	0.21	0.04	0.11
Cl[a]	12	0.19		0.68	0.93	0.27	0.80	0.34	0.44
K_2O[a]	25	1.03		1.88	3.06	1.33	3.54	1.95	3.07
CaO[a]	32	8.68		1.59	2.54	1.22	2.81	2.12	4.56
TiO_2[a]	46	0.11		0.45	0.71	0.26	0.69	0.39	0.57
MnO[a]	56	0.24		0.05	0.09	0.04	0.06	0.03	0.23
Fe_2O_3[a]	45	0.33		2.26	4.73	2.10	2.78	1.75	6.66
Li[b]	0.2		47.8	95	146	54	218	190	201
B[b]	0.90		623	3744	6047	2779	6670	5508	5837
Ti[b]				2649	4220	1428	4110	2919	3522
V[b]	0.12		38	38	55	21	47	31	36
Cr[b]	7		19	31	37	16	36	24	27
Co[b]	0.03		1434	5	6	3	5	4	4
Ni[b]	1.5		183	21	16	11	15	10	10
Cu[b]	0.4		9920	1085	16	115	17	66	17
Zn[b]	0.45		416	34	39	17	30	22	26
As[b]	1		27	67	22	910	37	20	14
Se[b]				n.d.	4	n.d.	n.d.	n.d.	n.d.
Rb[b]	0.1		87	38	62	26	66	54	64
Sr[b]	0.03		959	125	201	85	222	351	488

Y[b]	0.008		0.2	16	25	9	23	17	19
Zr[b]	0.007		40	150	250	71	232	158	199
Nb[b]	0.005		0.6	10	15	5	15	11	13
Mo[b]				1.10	1.40	0.49	0.97	0.45	0.52
Ag[b]	0.07		15.8	64.64	0.63	38.70	0.86	72.38	0.11
Sn[b]	0.9		1534	19201.4	44.5	31530.7	142.4	5887.3	3.0
Sb[b]	8		14098	136	bdl	342	bdl	55	bdl
Cs[b]	0.06		0.3	1.11	1.63	0.85	1.70	1.07	1.26
Ba[b]	0.055		4841	241.331	346.932	157.948	391.439	331.314	416.777
La[b]	0.004		0.33	15.437	23.593	7.783	21.116	13.471	16.336
Ce[b]	0.002		0.24	35.037	53.558	15.795	43.820	26.686	31.682
Pr[b]	0.001		0.03	3.590	5.428	1.733	4.755	3.006	3.661
Nd[b]	0.007		0.12	12.326	18.924	7.560	20.056	12.952	15.562
Sm[b]	0.007		0.03	2.565	3.929	1.529	4.047	2.735	3.327
Eu[b]	0.004		0.10	0.494	0.747	0.310	0.795	0.547	0.640
Gd[b]	0.007		0.04	2.396	3.701	1.500	3.761	2.532	3.045
Tb[b]	0.001		<0.01	0.414	0.637	0.216	0.537	0.385	0.456
Dy[b]	0.005		0.03	2.547	3.932	1.584	3.967	2.890	3.451
Ho[b]	0.001		<0.01	0.572	0.924	0.309	0.811	0.586	0.675
Er[b]	0.003		0.03	1.626	2.505	1.073	2.660	1.908	2.252
Tm[b]	0.006		<0.01	0.260	0.417	0.140	0.343	0.253	0.308
Yb[b]	0.001		0.03	1.657	2.664	1.038	2.694	2.000	2.347
Lu[b]	0.004		<0.01	0.270	0.441	0.138	0.369	0.273	0.302
Hf[b]	0.003		1.0	3.936	6.371	2.203	6.226	4.424	5.618
Pb[b]	1		717	204096	480	323003	2518	59854	26
Bi[b]	0.006		8.5	4.325	0.046	16.844	0.157	19.999	0.036
Th[b]	0.001		0.29	6.345	9.152	3.172	6.984	4.244	5.181
U[b]	0.005		0.18	2.296	3.191	0.966	2.479	1.295	1.502

Table 3: reduced oxide composition calculated following Panighello et al. (2012)

Number	Na_2O*	MgO*	Al_2O_3*	SiO_2*	P_2O_5*	K_2O*	CaO*	Fe_2O_3*
Sa-01y	18.10	1.14	8.53	64.02	0.20	2.63	2.23	3.17
Sa-01b	22.26	1.29	9.73	55.84	0.21	3.17	2.63	4.89
Sa-02y	16.38	0.67	6.81	68.99	0.17	2.00	1.84	3.15
Sa-02b	21.96	1.38	10.70	56.14	0.28	3.70	2.93	2.91
Sa-03y	17.17	0.65	8.89	66.04	0.15	2.38	2.59	2.13
Sa-03b	20.54	0.95	9.21	54.41	0.21	3.16	4.68	6.84

Table 4: Sr, Pb and B isotopic analysis of the samples, standard deviations are based on 3 repeat measurements, n.d. are samples for which the ratios were not determined.

Number	$^{87}Sr/^{86}Sr$	2σ	$^{208}Pb/^{204}Pb$	2σ	$^{207}Pb/^{204}Pb$	2σ	$^{206}Pb/^{204}Pb$	2σ	$^{208}Pb/^{206}Pb$	2σ	$^{207}Pb/^{206}Pb$	2σ	$\delta^{11}B$	2σ
Sa-01y	n.d.	n.d.	38.640	0.023	15.648	0.009	18.544	0.010	2.0830	0.0001	0.84382	0.00001	n.d.	n.d.
Sa-01g	0.71809	0.00012	n.d.		n.d.		n.d.		n.d.		n.d.		0.2	0.2
Sa-02y	n.d.	n.d.	38.561	0.023	15.664	0.009	18.382	0.010	2.0979	0.0001	0.85706	0.00001	n.d.	n.d.
Sa-02b	0.71634	0.00088	n.d.		n.d.		n.d.		n.d.		n.d.		n.d.	n.d.
Sa-03y	n.d.	n.d.	38.630	0.226	15.525	0.010	18.737	0.127	2.062	0.002	0.8286	0.0004	0.7	0.3
Sa-03b	0.71756	0.00072	n.d.		n.d.		n.d.		n.d.		n.d.		n.d.	n.d.

Table 5: comparison of alkali ratios between the glasses and hot springs in the vicinity of Sardis

Sample	Na/K	Na/Mg	K/Mg	Na/B
High-boron glasses from Sardis				
Sa-01y	6.2	19.6	3.2	25.6
Sa-01bl	6.3	21.2	3.4	26.4
Sa-02y	7.3	29.9	4.1	29.1
Sa-02bl	5.3	19.6	3.7	23.4
Sa-03y	6.5	32.4	5.0	19.0
Sa-03bl	5.8	26.6	4.6	25.4
Hot spring waters of the Na-HCO_3 type in the vicinity of Sardis (Vengosh et al., 2012)				
Urganli	10.4	37.1	3.6	57.1
Salini	6.3	11.2	1.8	11.6
Salini	5.8	29.2	5.0	10.6

S1: Geographical location of the archaeological site Sardis, other places mentioned in this article are also included.

Supplemental Information

Materials and Archaeological context

The beads analyzed here were found in Iron Age contexts in excavation sectors on the west side of the Lydian city, where most excavation has been concentrated. Samples Sa-1, Sa-2, and Sa-3 were excavated at sector MMS, a sector aimed at understanding the western fortification of Sardis (S2, S3). This fortification, built in the late seventh or early sixth century BCE, was fully 20 m wide at the base, and for much of its length still stands 10-12 m high. The wall was further strengthened with a massive glacis, a ramped earthwork built of layers of artificial imported fill piled against the outer face of the fortification, which more than doubled the width of the original wall. "Recesses" or gaps in the glacis framed by retaining walls served some uncertain, presumably military purpose. One of these recesses was the findspot of three Lydian coins (Cahill and Kroll, 2005).

S2. Plan of Fortification Sector MMS.

S3. Section through the Lydian Fortification showing earlier fortification and findspots of beads samples 1-3

This structure was not, however, the earliest fortification of the lower city. Underneath and almost completely buried by the colossal wall is an earlier, smaller structure, almost certainly a predecessor fortification. A probe to investigate this early feature was dug in 2008 and 2009 on the shoulder of the Izmir-Ankara highway, where road construction in the 1950s had destroyed much of the mudbrick superstructure of the later fortification (S4; Cahill, 2010b; Cahill, 2011). Removal of the remaining mudbrick and the stone socle exposed a small area of the earlier fortification and occupation levels predating this earlier phase. A massive stone wall parallel to the later fortification is probably the first phase of this early fortification. Its western, outer face was later buried by an artificial land fill, which was retained on the north by a stone feature at roughly a right angle to the wall face. We currently interpret this situation as similar to the later (and also incompletely understood) fortification: an original wall face (here stone rather than mudbrick), which was deliberately enlarged with a glacis of artificial fill, retained by a retaining wall which may have marked another recess or a gate.

S4. Plan of sondage beneath the Lydian Fortification, showing earlier fortification and findspots of beads samples 1-3.

Two of the beads analyzed, Sa-1 and Sa-2, were found in the artificial fill or glacis laid against the earlier fortification. A third, larger biconical bead with two yellow wavy trails and dots at the midpoint was found in this same context but could not be sampled (G08.002). The latest pottery from this fill included local Lydian and imported Greek ceramics dating to the seventh century BCE, probably no earlier than the middle of the century. Diagnostic sixth century wares and shapes are noticeably absent. Since all these features were sealed by the solid construction of the later fortification, dated to the late seventh or earlier sixth century BCE, a terminus ante quem of approximately 600 BC is assured. Their context in layers of artificial, imported fill, however, leaves open the possibility that these date to rather earlier than the second half of the seventh century, and are residual in this later context.

The third bead, Sa-3, was found in a deeper stratum predating this early fortification. A series of earth floors running under the early fortification probably reflect domestic occupation here; an ashy pit cut into these also predates the early fortification. The small amount of local pottery found in these levels was not closely datable, but a date in the late eighth or early seventh century seems most probable.

A fascinating but possibly coincidental discovery nearby is the remains of a Lydian domestic workshop where opaque red cuprite glass and other materials were being worked. Some 4.8 kg of red glass cullet and 0.5 kg. of transparent yellowish glass cullet, as well as a few worked objects and tools were found in one room of a house just inside the fortification wall; the room was equipped with two benches, perhaps for working glass and possibly other materials (Brill and Cahill, 1988). The workshop was part of a house, which in its final form was built in the first half of the sixth century BCE and destroyed, with the fortification, by Cyrus in about 547 BCE. Earlier phases of the house walls and floors, however, date to the seventh century BC and are probably contemporary with the earlier phase of the fortification. No glass artifacts were found in these early levels of the house, and it may simply be coincidence that glass was being worked in this area of Sardis, a century or so after the glass beads here discussed.

The fourth bead, Sa-4, is the earliest of the beads sampled in this study, and probably the earliest of this type from Sardis. It was recovered in 1962 during the excavation of "Deep Sounding B" in sector HoB, outside the city walls (S5; context: Hanfmann, 1963, 4-6; Ramage et al., 2018; von Saldern, 1980, no. 830). "Deep Sounding B" was one of three sondages into Early Iron Age levels in this sector. This sondage was begun from a destruction level dated to the last quarter of the eighth century BCE (Ramage, 1994; Ramage et al., 2018). The bead was found in fill more than a meter below the destruction level. Because the rate of deposition of the sand and gravel is uncertain and variable, we can only estimate the date of the context, but it is likely to be in the first half of the eighth century BCE.

S5. View of sondage, 2009

References SI

Cahill ND, Kroll JH (2005) New Archaic Coin Finds at Sardis. *American Journal of Archaeology* 109 (4): 589-617.

Brill RH, Cahill ND (1988) A red opaque glass from Sardis and some thoughts on red opaques in general. *Journal of Glass Studies* 30: 16-27.

Cahill ND (2010b) Sardis, 2008. *Kazı Sonuçları Toplantısı* 31: 63-78.

Cahill ND (2011) Sardis, 2009. *Kazı Sonuçları Toplantısı* 32: 358-367.

Hanfmann GMA (1963) The Fifth Campaign at Sardis (1962). *BASOR* 170: 1-65.

Ramage A (1994) Early Iron Age Sardis and its Neighbours. In *Anatolian Iron Ages 3. The proceedings of the Third Anatolian Iron Ages Colloquium Held at Van, 6-12 August 1990*, eds Çilingiroğlu A, French DH (British Institute of Archaeology, Ankara).

Ramage A, Ramage NH, Gürtekin-Demir RG. Forthcoming. *House of Bronzes Lydian Trench: Final Report*. Sardis Report.

von Saldern A (1980) Ancient and Byzantine Glass from Sardis. *Archaeological Exploration of Sardis Monograph 6* (Harvard University Press, Cambridge, Massachusetts).

S2. Plan of Fortification Sector MMS.

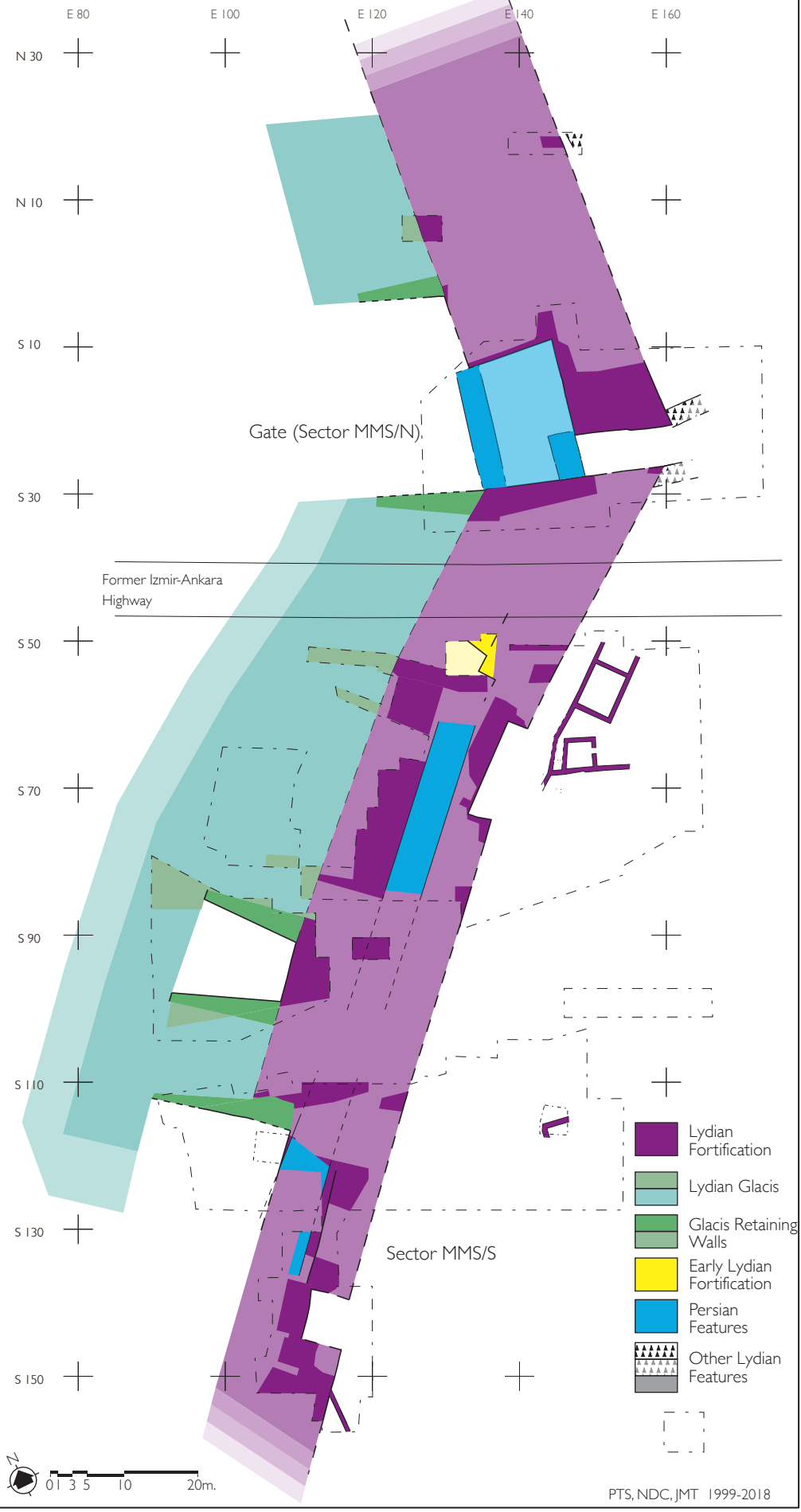

S3. Section through the Lydian Fortification showing earlier fortification and findspots of beads samples 1-3

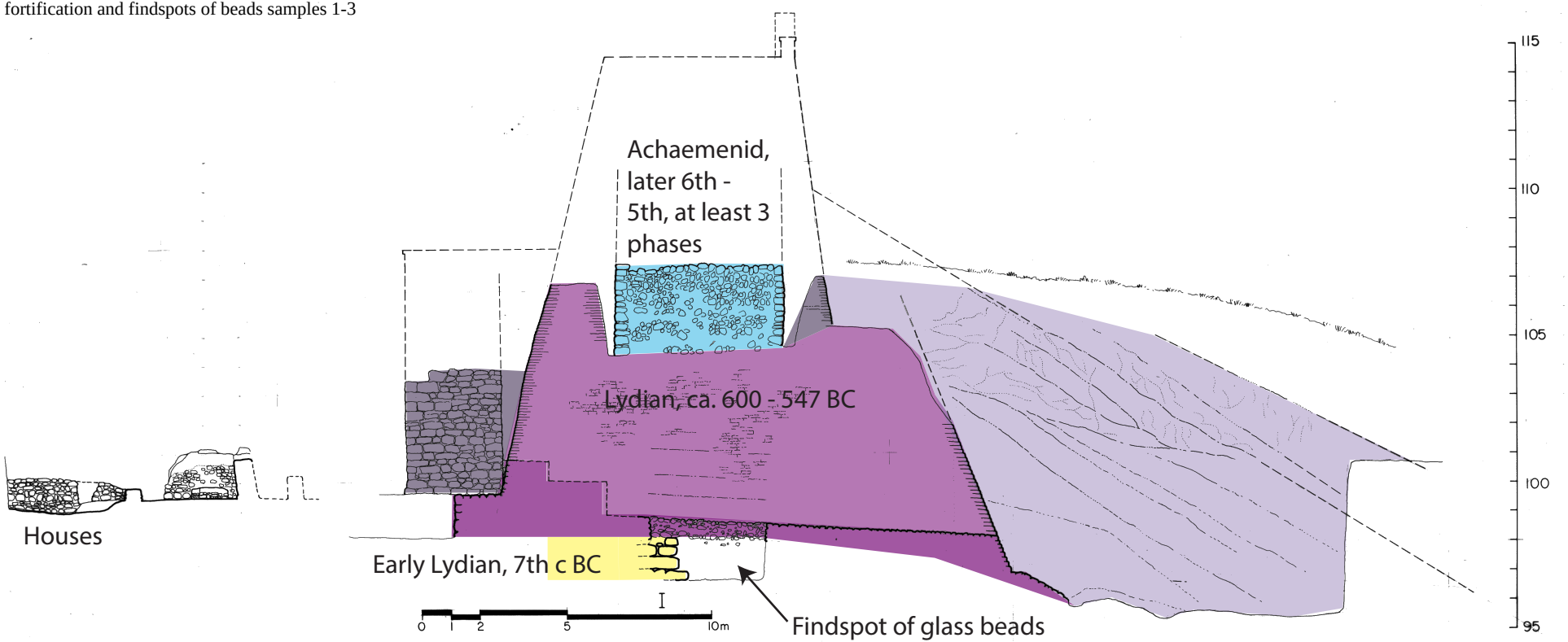

S4. Plan of sondage beneath the Lydian Fortification, showing earlier fortification and findspots of beads samples 1-3.

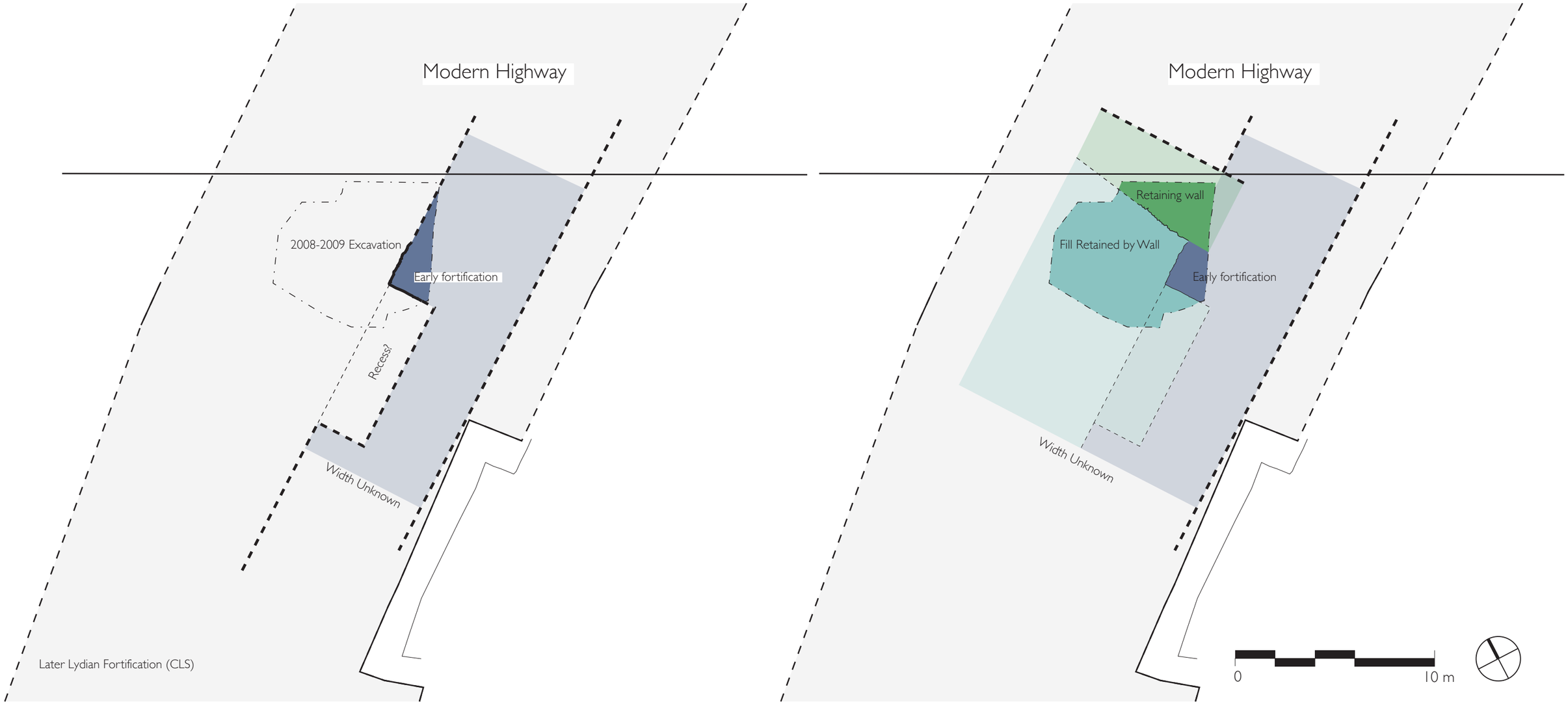

SECTOR MMS: HYPOTHETICAL RECONSTRUCTION OF EARLY LYDIAN FORTIFICATION

NDC 2009

S5. View of Sondage, 2009

Map - Sardis


Black Sea
N
Varna
Sofia
BULGARIA
Prishtina
KOSOVO
Podgorica
MONTENEGRO
Skopje
MACEDONIA
ALBANIA
Tiranë
Thessaloniki
Istanbul
Sea of Marmara
Bursa
Eskisehir
Samsun
KUZEY ANADOLU DAGLARI
Sivas
Ankara
Pergamon
Sardis
TURKEY
Kayseri
Elazig
Tuz Gölu
Izmir
Malatya
Diyarbakir
Konya
TAURUS MOUNTAINS
Adana
Gaziantep
Antalya
Mersin
Aleppo
Euphrates
Aegean Sea
GREECE
North Aegean Trough
Athens
Ionian Sea
Sea of Crete
Hellenic Trench
Crete
Cretan-Rhodes Ridge
Antalya Basin
NORTHERN CYPRUS
CYPRUS
Lefkosia (Nicosia, Lefkoşa)
Cyprus
Hims
SYRIA
LEBANON
Beirut
Damascus
Herodotus Trough
Herodotus Basin
Beirut Escarpment
Haifa
Tel Aviv-Yafo
Nile Fan
Banghazi
Tobruk
Amman
Ghazzah (Gaza City)
GAZA STRIP
0
180
360
720 Kilometers
National Geographic, Esri, Garmin, HERE, UNEP-WCMC, USGS, NASA, ESA, METI, NRCAN, GEBCO, NOAA, increment P Corp.